A Numerical Study on the Impact of Hygroscopic Seeding on the Development of Cloud Particle Spectra

Dimitri Caro, Wolfram Wobrock, Andrea Flossmann

A Numerical Study on the Impact of Hygroscopic Seeding on the Development of Cloud Particle Spectra

DIMITRI CARO, WOLFRAM WOBROCK, AND ANDREA I. FLOSSMANN

Laboratoire de Météorologie Physique, Université Blaise Pascal-CNRS-OPGC, Aubière, France

(Manuscript received 27 December 2000, in final form 3 September 2001)

ABSTRACT

In a detailed microphysical model embedded into a parcel dynamics, a number of sensitivity studies were effected to test hygroscopic seeding of warm and mixed-phase clouds, varying the size distribution and total number of salt particles. For *warm* clouds in general, earlier results in the literature could be confirmed. More specifically the following conclusions were reached: Certainly, from practical considerations (weight, easy handling), hygroscopic flares have advantages with respect to earlier hygroscopic seeding techniques. The modeling study supports this choice. Smaller seeding particles have the advantage of increasing the number of drizzle-size drops, which increases the chance of the seeding material staying in the cloud and affecting the entire cloud. Larger salt crystals, though increasing precipitation production in the model, risk premature precipitation fallout. The competition between natural and seeding particles was studied. Concerning the number concentration of the seeding agents, it seems that increasingly higher number concentrations result in a kind of saturation of the seeding effect, not further improving rain formation. Mean radii between 0.5 and 6 μm seem to be the optimum to get a maximum seeding effect. Concerning the *mixed*-phase clouds, the same kinds of sensitivity tests concerning the seeding agents, their size distributions, and their number concentrations were performed. As in warm clouds, hygroscopic seeding in mixed-phase clouds modifies the collision and coalescence process. The formed drops freeze, leading to the formation of numerous graupel particles between 1- and 9-mm radius, while depleting the liquid phase. The small ice crystals remained almost unaffected.

1. Introduction

Each year, devastating hailfalls cause much damage to the agricultural community (e.g., Morgan 1973). Thus, much research aimed at the better understanding of the production of hail, improved forecasting, and possible hail prevention has been done during the 1970s and 1980s, but no conclusive results have been found (Foote and Knight 1979). During these studies seeding agents such as AgI or dry ice were used in seeding trials. These were intended to increase the number of small ice nuclei, which, then, share among themselves the available supercooled water and, thus, reduce the size of the formed hail stones. The Russian scientific community has claimed to have successfully reduced hail production through cloud seeding (Sulakvelidze and Tsykunov 1974), but other studies such as the National Hail Research Experiment in the United States (Knight and Squires 1982), or the Grossversuch IV in Switzerland (Federer et al. 1986) have not been able to reproduce their findings. In all non-Russian campaigns the seeding results remained inconclusive and statistically not significant. Research in this field became rare over the following years. However, a certain impact was reported concerning inadvertent seeding of clouds by ship tracks or forest fires (e.g., Ackerman et al. 1995). Then, Mather (1991) reported a result of inadvertent seeding by hygroscopic particles emitted from a Kraft paper mill. This observation led to further cloud seeding experiments in South Africa and elsewhere, aimed at rainfall enhancement, which seemed to produce encouraging results. Work by Mather et al. (1997), for example, indicated a positive relationship between seeded clouds and increased rainfall intensities for convective clouds using hygroscopic salt nuclei generated by pyrotechnic flares. Furthermore, the discovery of the technique of hygroscopic flares, which have certain advantages with respect to the classical seeding techniques with salt particles, in terms of weight and handling, gave a fresh impulse to the domain and encouraged researchers to reconsider the possibility of hygroscopic cloud seeding to modify the evolution of clouds.

Numerical models provide an interesting tool for studying possible effects of seeding, without having to run a costly campaign. A number of modeling studies using spectral microphysics have already looked at the problem from a theoretical point of view. Here, we want to mention especially the modeling work pre-

Corresponding author address: Andrea I. Flossmann, Laboratoire de Météorologie Physique, Université Blaise Pascal-CNRS-OPGC, 24 avenue des Landais, Aubière Cedex 63177 France.
E-mail: a.flossmann@opgc.univ-bpclermont.fr

sented by Cooper et al. (1997; hereinafter CBM97), Tzivion et al. (1994; hereinafter TRL94), and Silverman and Sukarnjanaset (1996; hereinafter SS96). Furthermore, work on this subject has been done by, among others, Reisin et al. (1996; hereinafter RTL96), and Yin et al. (2000; hereinafter YLRT00). They all investigated the hygroscopic seeding with particles ranging in size from giant salt particles to small particles around 0.5 μm created by hygroscopic flares.

The models, apart from employing a spectral microphysics concept, were quite different. CBM97 used a Lagrangian parcel dynamics model, SS96 an Eulerian one- and one-half-dimensional model, TRL94 and RTL96 an Eulerian three-dimensional, axisymmetric model, and YLRT00 an Eulerian two-dimensional, slab-symmetric model. Thus, it is difficult to compare quantitatively, as well as qualitatively, the results obtained. Furthermore, most of the investigations (except CBM97) focused on the change of the precipitation on the ground and radar reflectivity, without putting much attention on the evolution of the hydrometeor spectra inside cloud and the change induced in these spectra due to seeding. The current study focuses on this point.

In the past we have developed the ''detailed scavenging and microphysical'' model (DESCAM). Originally this model served to study scavenging of gases and particles by clouds and has already been applied to a number of case studies. This model contains prognostic equations for the number density distribution function of aerosol particles in air. In addition, it can distinguish between different types of aerosol particles serving as condensation nuclei and, thus, allows studying the possible competition among nuclei of different origin. Consequently, the size dependency of the seeding agents is treated more explicitly than in the modeling exercises quoted above, which only consider a dependency of the type CS^k for the number of cloud condensation nuclei (CCN), as a function of supersaturation. Furthermore, DESCAM contains a spectral representation of the ice microphysics, that is, for small ice crystals and graupel particles.

In order to simplify the investigation of the changes in hydrometeor spectra due to seeding, our microphysical model is embedded in a simple parcel dynamics. This approach imposes certain restrictions on the interpretation of the results. A parcel model can only simulate the initial phase of a cloud where ascending air motion is dominant over any particle-settling effects. Thus, the evolution of liquid and solid precipitation cannot be studied. Equally, the spectral ice microphysics treats the graupel phase of the cloud up to the achievement of a graupel diameter of 18 mm. Hailstone production is not included. Consequently, we will use the model to study the change in liquid and solid hydrometeor spectra due to the seeding with hygroscopic salt particles of different size spectra during the early lifetime of a cloud. In this sense it presents an extension of the work of CBM97 to additional sensitivity studies concerning the warm case and an extension of the approach in general to mixed-phase clouds. Thus, the study, and a comparison with some of the modeling studies mentioned above, allows one to resolve some stated discrepancies in literature and to indicate possible impacts of hygroscopic flares on mixed-phase clouds. One aspect of the study will concern the number of drizzle-sized drops formed due to seeding. Even though this has not been confirmed by measurements yet, there exists a theory in the literature (see e.g., CBM97) that increasing the number of drizzle-sized drops increases the chance of the seeding material to stay in the cloud and to affect the whole cloud. Larger salt crystals, though increasing precipitation production in the model, risk premature precipitation. Other theories indicate that hygroscopic seeding might be mainly acting through dynamical effects. This aspect cannot be addressed with a parcel model. However, it is possible to study the impact of the seeding techniques on the production of drizzle-sized particles, without judging whether or not they will play the role they are suspected of playing, in real clouds.

In the first section of this paper we will present the model used. In the second section we will apply the model to hygroscopic seeding in warm clouds. We reapply different approaches from the literature to initialize seeding in order to homogenize the results, compare them to the original work and extend them to further sensitivity studies. In the third section we will apply all three approaches to mixed-phase cloud in order to study the potential of the hygroscopic seeding for modifying such clouds.

2. The model architecture

a. The air parcel dynamics

For studying cloud evolution, air parcel models represent the simplest dynamics possible. They are able to represent the early stages of cloud formation, where cloud-free, buoyant parcels rise from the surface and reach saturation. This represents the level of cloud base. Due to the condensation process, latent heat is released, maintaining buoyancy. The cloudy parcel continues to rise and the hydrometeors evolve. They grow via condensation, collide and coalesce and break up if they become too large. When the temperature decreases below 0°C an ice phase is initiated. Eventually, when the temperature gradient between the parcel and the environment no longer support vertical motion, the parcel comes to rest.

Thus, air parcels are a valid tool for studying the early phases of cloud formation. They even allow studying the initiation and formation of precipitating hydrometeors inside the parcel. However, due to the quasi-closed concept of air parcels, no sedimentation of precipitation-

TABLE 1. Ten density distribution functions are used in the DESCAM model with m being the drop mass, m_{AP} being the total aerosol particle mass; k represents different chemical composition of particles ($k = 1$ is background aerosol particles, $k = 2$ is seeded particles), m_i being the ice crystal mass, and m_g being the graupel mass; the drop and aerosol particle, the ice crystal, and graupel particle categories are logarithmically equally spaced with a mass doubling every second category.

$f_d(m)$	Drop number density distribution function.	69, 1–2580 μm
$g_{APd,k}(m)$	Mass density distribution function for aerosol. Particles in the drops having the chemical composition k.	69, 1–2580 μm
$f_{APa,k}(m_{AP})$	Aerosol particle number density distribution. Function for particles of chemical composition k in the air.	107, 10^{-3}–200 μm
$g_{APa,k}(m_{AP})$	The mass density distribution function for aerosol particles of chemical composition k in the air.	107, 10^{-3}–200 μm
$f_i(m_i)$	Number density distribution function for hexagonal ice crystals.	69, 1–2580 μm
$g_i(m_i)$	Mass density distribution function for hexagonal ice crystals.	69, 1–2580 μm
$g_{APi,k}(m_i)$	Mass density distribution function for aerosol particles in hexagonal ice crystals of chemical composition k.	69, 1–2580 μm
$f_g(m_g)$	Number density distribution function for graupel particles.	40, 90–9000 μm
$g_g(m_g)$	Mass density distribution function for graupel particles.	40, 90–9000 μm
$g_{APg,k}(m_g)$	Mass density distribution function for aerosol particles in graupel particles of chemical composition k.	40, 90–9000 μm

sized hydrometeors can be considered. Thus, their applicability ends when, in real clouds, precipitation starts falling measurably with respect to the air, and downdrafts develop next to the updraft core.

The evolution of temperature T, vertical wind speed W, and moisture w_v inside a rising and entraining air parcel can be calculated by (Pruppacher and Klett 1997; Flossmann et al. 1985):

$$\frac{dW}{dt} = \frac{g}{1+\gamma}\left(\frac{T_V - T'_V}{T'_V} - w_L\right) - \frac{\mu}{1+\gamma}W^2,$$

$$\frac{dT}{dt} = -\frac{gW}{c_p} - \mu(T - T')W + \frac{L_e}{c_p}C_{\mathrm{Ph},e} + \frac{L_m}{c_p}C_{\mathrm{Ph},m} + \frac{L_s}{c_p}C_{\mathrm{Ph,s}}, \quad \text{and}$$

$$\frac{dw_v}{dt} = -\mu(w_v - w'_v) - C_{\mathrm{PH},e} - C_{\mathrm{PH},s},$$

where g is the acceleration of gravity; $\gamma \sim 0.5$; w_L is the liquid water content; μ is the entrainment rate; c_p is the specific heat of air at constant pressure; L_e, L_m, and L_s are latent heat of evaporation, melting, and fusion, respectively; and, $C_{\mathrm{PH},e}$, $C_{\mathrm{PH},m}$, and $C_{\mathrm{PH},s}$ are rates of evaporation, melting, and fusion, respectively. The primed quantities pertain to the values in the environment. The entrainment rate can be parameterized using the assumption of a homogeneous entrainment, as in Pruppacher and Klett (1997):

$$\mu = \frac{\alpha}{R},$$

where

$$\frac{d\ln R}{dt} = \frac{1}{3}\left(\mu W - \frac{d\ln\rho}{dt}\right),$$

where ρ is the density of the air. The homogeneous entrainment approach has limitations; for example, Baker and Latham (1979, 1982) and Baker et al. (1980) suggest that in clouds an inhomogeneous mixing is effective. However, in the present study, which is not aimed at realistically modeling the lifecycle of a cloud, but rather intended to study possible effects of the seeding approach, using homogeneous entrainment will probably be sufficient. The effect of different values for α, ranging from $\alpha = 0$ (adiabatic case) to $\alpha = 0.9$ will be discussed below.

b. The microphysics model

The basic microphysical framework employed in the present study is the model DESCAM, as discussed in Flossmann et al. (1985, 1987). There, the aerosol particles are treated in a spectral form. Apart from adiabatic lifting and entrainment–detrainment, the number of particles of a certain size changes due to activation of droplets, size changes resulting from humidity changes, and impaction scavenging by drops. The nucleated drops then grow by condensation or evaporate, collide, and coalesce, and eventually break up. During their lifetime they further scavenge particles, and the scavenged pollutant mass is redistributed through the microphysical processes. The extension of this microphysical and scavenging model to the scavenging of two different types of aerosol particles [e.g., $(NH_4)_2SO_4$ and NaCl for marine air masses] is described in Flossmann (1991) and the inclusion of effects of gaseous H_2O_2 and O_3 on the uptake and oxidation of SO_2 was presented in Flossmann (1994).

In its extension to mixed-phase clouds the model DESCAM (Alheit et al. 1990) considers additionally the number and mass density distribution functions of ice crystals assumed as hexagonal plates and graupel particles, as well as the aerosol mass attached to them. The

distribution functions used in the present application are summarized in Table 1. The main process to initialize ice formation in this model is the Bigg drop-freezing process (Bigg 1953):

$$\frac{dN_f}{dt} = N_d B' V_d \exp[b'(T_0 - T)],$$

as used in Orville and Kopp (1977). Herein, N_f is the number of frozen drops, N_d is the number of unfrozen drops of volume V_d, and $T_0 = 273$ K.

Alheit et al. (1990) showed that the Bigg freezing process dominates the formation of large ice particles over the vapor deposition on Fletcher ice nuclei, in convective clouds. Furthermore, we did not consider the Hallet–Mossop ice multiplication process [for details see Pruppacher and Klett (1997)] which increases the number of ice crystals and, thus, slows down the development of large ice aggregates. Our study focuses on the initial phase of the hail development, where the ice aggregates just begin to form. Consequently, the graupel size distribution ends at 9 mm in radius, which is just the beginning of the hail sizes. In order to simulate hail production correctly, a complete dynamical framework is necessary.

Thus, the considered density distribution functions obey to a prognostic equation of the form:

$$\begin{aligned}
\frac{\partial \psi(m)}{\partial t} = {} & -\mu[\psi(m) - \psi'(m)]U && (d, i, g, \text{AP}),\\
& + \left.\frac{\partial \psi(m)}{\partial t}\right|_{\text{(activation/deactivation of drops)}} && (d, \text{AP}),\\
& + \left.\frac{\partial \psi(m)}{\partial t}\right|_{\text{(nucleation of ice crystals)}} && (i, \text{AP}),\\
& + \left.\frac{\partial \psi(m)}{\partial t}\right|_{\text{(freezing of drops} \rightarrow \text{ice crystals/graupel)}} && (d, i, g),\\
& + \left.\frac{\partial \psi(m)}{\partial t}\right|_{\text{(condensation/evaporation)}} && (d, i, g, \text{AP}),\\
& + \left.\frac{\partial \psi(m)}{\partial t}\right|_{\text{(impaction scavenging)}} && (d, i, g, \text{AP}),\\
& + \left.\frac{\partial \psi(m)}{\partial t}\right|_{\text{(collision and coalescence)}} && (d),\\
& + \left.\frac{\partial \psi(m)}{\partial t}\right|_{\text{(breakup)}} && (d),\\
& + \left.\frac{\partial \psi(m)}{\partial t}\right|_{\text{(riming of ice crystals and graupel)}} && (d, i, g),\\
& + \left.\frac{\partial \psi(m)}{\partial t}\right|_{\text{(conversion ice crystals} \rightarrow \text{graupel)}} && (i, g), \quad \text{and}\\
& + \left.\frac{\partial \psi(m)}{\partial t}\right|_{\text{(melting of ice crystals and graupel)}} && (d, i, g),
\end{aligned}$$

where d indicates the terms appearing in the equation for the drops, i those for the hexagonal ice crystals, g those for the graupel, and AP those for the aerosol particles in air.

3. The initialization of the model

a. Initialization of dynamics and thermodynamics

The air parcel is initialized with a radius of 350 m

TABLE 2. Parameters for the background rural aerosol particle distribution for the air parcel dynamics; n_i = total number of aerosol particles per cubic centimeters; R_i = geometric mean aerosol particle radius (μm); σ_i = std dev in mode i.

Mode i	n_i	R_i	log σ_i
1	6650	0.007 39	0.225
2	147	0.0269	0.557
3	1990	0.0419	0.266

TABLE 3. Parameters for the seeding aerosol particle distribution after CBM97, TRL94, and SS96 for the air parcel dynamics; n_i = total number of aerosol particles per cubic-centimeter; R_i = geometric mean aerosol particle radius (μm); σ_i = std dev in mode i.

Case after	Mode i	n_i	R_i	logΣ_i	Model case
CBM97	1	150	0.15	0.2	C4
	2	0.105	0.5	0.4	
TRL94	1	3.1×10^{-3}	16	0.08	T2
SS96	1	1.3×10^{-4}	113	0.6	S

and is launched at an initial altitude corresponding to cloud base of 1000 m for the study of warm clouds and at 750 m for the study of mixed-phase clouds. The temperature and pressure values are those of the prescribed environmental sounding. The relative humidity is set to 99% and the initial vertical velocity to 1 m s^{-1}, a typical value for cumulus clouds. The different cloud base is due to the different soundings used for warm and for mixed-phase clouds: For the warm-cloud case the sounding is the one described by Lee et al. (1980) and for the mixed-phase clouds the sounding is the one described by Alheit et al. (1990).

b. Initialization of the aerosol particle spectrum

1) INITIALIZATION OF THE BACKGROUND AEROSOL PARTICLE SPECTRUM

The initial dry aerosol particle spectrum for the background was assumed to be of rural type consisting of a superposition of three lognormal distributions as proposed by Jaenicke (1988):

$$\frac{dN}{d\ln r} = f_{APa}(\ln r) = \sum_{i=1}^{3} \frac{n_i}{(2\pi)^{1/2}\log\sigma_i \ln 10} \exp\left\{-\frac{[\log(r/R_i)]^2}{2(\log\sigma_i)^2}\right\}. \quad (1)$$

The parameters are summarized in Table 2. In order to simplify the calculations, all particles were assumed to consist of 100% $(NH_4)_2SO_4$.

The resulting dry aerosol particle number size distribution is displayed in Fig. 1a. We selected this aerosol size distribution as it provides numerous cloud condensation nuclei during cloud formation. These CCN result in a narrow drop spectrum, containing about 850 cm^{-3} small drops immediately at cloud base. These grow only little during the ascent of the air parcel so that precipitation-sized drops form only very late. In general, this represents a cloud which is not very favorable for the formation of rain in a nonseeded case (cf. section 4). We chose this background spectrum, as our sensitivity tests confirmed the previous results of CBM97, TRL94, and SS96 that seeding is not very effective for a particle

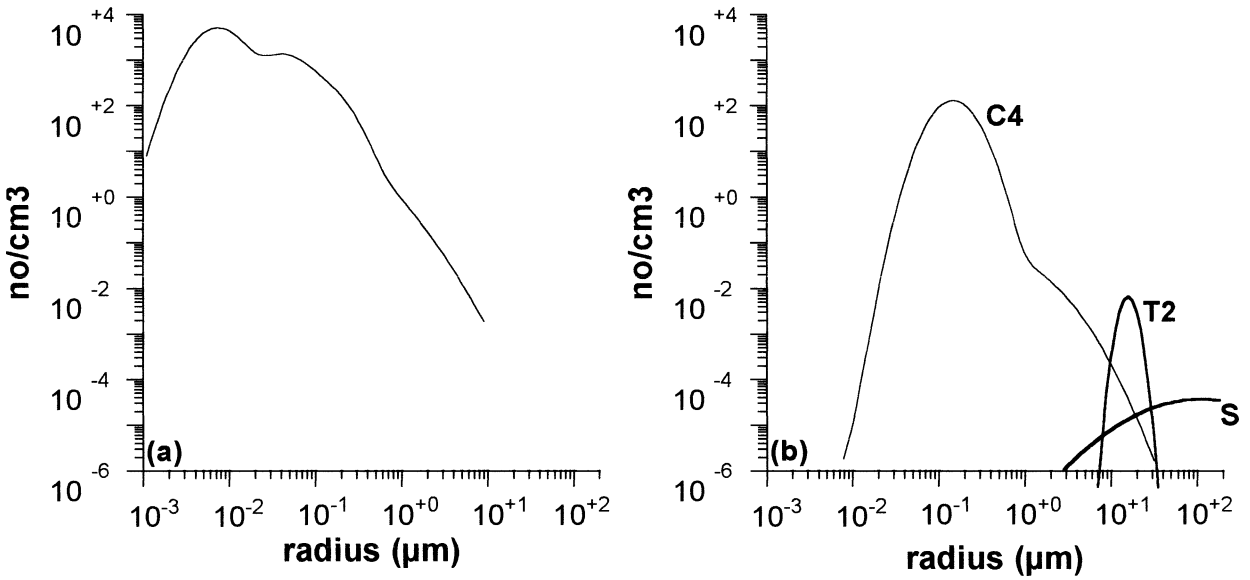

FIG. 1. (a) Initial dry number density distribution function of the background aerosol particle spectrum as given by Eq. (1) and Table 2. (b) Initial dry number density distribution function of the seeding aerosol particle spectrum after CBM97 (C4), TRL94 (T2), and SS96 (S).

spectrum, such as a marine aerosol particle spectrum, that produces rain on its own.

2) Initialization of the seeding spectrum

In order to simulate the seeding of a cloud by hygroscopic particles in the model, we add to the dry background aerosol particle spectrum a second aerosol particle spectrum resulting from the seeded salt nuclei. As explained earlier, seeded particles can have a variety of different sizes. We have focused here on three different size ranges, each one taken from a publication concerned with the simulation of a seeding event. Due to the fact that we use the same kind of model for the different seeding approaches it will be possible to compare at least qualitatively the effect of the different seeding methods. However, we will disregard the fact that the different seeding techniques are used differently at different cloud altitudes, in real clouds. In the present study all seeding agents will be injected below cloud base to keep the results comparable.

(i) Cloud seeding after Cooper et al.

The study made by CBM97 and part of the study by SS96 is based on the seeding technique using hygroscopic flares. Investigations by Mather et al. (1997) showed that the salt particles are relatively small. Following CBM97 we approximated the seeded spectrum by a superposition of two lognormal modes (No. mod = 2):

$$\frac{dN}{d\ \ln r} = f_{\mathrm{APa}}(\ln r) = \sum_{i=1}^{\text{No. mod.}} \frac{n_i}{(2\pi)^{1/2}\ \log\sigma_i\ \ln 10} \exp\left\{-\frac{[\log(r/R_i)]^2}{2(\log\sigma_i)^2}\right\}. \quad (2)$$

The mean radius and the standard deviation of the two lognormal modes were taken as proposed by CBM97 and are summarized in Table 3. The seeding particles were assumed to consist entirely ($\varepsilon = 1$) of NaCl, for all seeding spectra used in this modeling exercise. Obviously, hygroscopic particles can also be made of calcium chloride or other salts. However, for the configuration chosen, the role of the chemical composition is not dominant. In the parcel model, at $t = 0$ s, the aerosol particles are assumed to be wet and at equilibrium size with 99% relative humidity. Sensitivity tests (Ahr et al. 1989) have shown that highly soluble aerosol particles ($\varepsilon > 0.5$) have taken up so much water at this stage that their solute concentration becomes negligible. Selecting NaCl will, thus, only affect the solute effect in the Köhler equation for lower relative humidities (Pruppacher and Klett 1997), having small impact on the number of particles activated. The resulting dry aerosol particle spectrum is displayed in Fig. 1b.

CBM97 also gave a ratio for the number concentration of each mode, which we maintained for our sensitivity test. For some sensitivity studies we will further follow CBM97 and just use one single mode with a standard deviation of 0.2. The cases studied with the seeding approach of CBM97 are summarized in Table 4.

TABLE 4. Test cases studied for the seeding after CBM97 and TRL94; n_i = total number of aerosol particles per cubic centimeter; R_i = geometric mean aerosol particle radius (μm); σ_i = std dev in mode i.

Case	n_1	n_2	R_1	R_2	$\log\sigma_1$	$\log\sigma_2$
C1	2600	1.82	0.15	0.5	0.2	0.4
C2	1500	1.05	0.15	0.5	0.2	0.4
C3	750	0.525	0.15	0.5	0.2	0.4
C4	150	0.105	0.15	0.5	0.2	0.4
C5	15	0.0105	0.15	0.5	0.2	0.4
C6	150		0.15		0.2	
C7	150		0.5		0.2	
C8	150		1.25		0.2	
T1	0.031		16		0.08	
T2	3.1×10^{-3}		16		0.08	
T3	3.1×10^{-4}		16		0.08	
T4	3.1×10^{-5}		16		0.08	
T5	3.1×10^{-3}		6		0.08	
T6	3.1×10^{-3}		10		0.08	
T7	3.1×10^{-3}		13		0.08	
T8	3.1×10^{-3}		20		0.08	

(ii) Cloud seeding after Tzivion et al.

The particles modeled by TRL94 are larger than those studied by CBM97, as they do not describe flares but rather hygroscopic particle seeding with a size around 16 μm. From the information given we derived an initial number concentration. Using a lognormal distribution with a single mode [No. mod. = 1 in Eq. (2)] our reference values are given in Table 3.

The resulting seeding spectrum (NaCl, $\varepsilon = 1$) is also displayed in Fig. 1b. The sensitivity tests effected with this seeding approach are summarized in Table 4.

(iii) Cloud seeding after Silverman and Sukarnjanaset

The last seeding approach we tested with our model represents the hygroscopic seeding method using very large salt crystals following one of the approaches of SS96. We have modeled this technique, as in the previous case, by one mode, using No. mod. = 1 in Eq. 2. Our reference values are given in Table 3 and the corresponding spectrum is included in Fig. 1b. We have done no sensitivity tests for this case.

4. Results of the sensitivity test for warm clouds

The first test we effected concerns the different seeding techniques modeled by CBM97, TRL94, and SS96 and how they perform with respect to the unseeded warm cloud. The characteristic features of the different

TABLE 5. Results for warm clouds for the test cases detailed in Table 4. In the cases where no value for α is indicated, $\alpha = 0.6$ was used. The number concentrations of drops N_d as function of time, and the activated aerosol particles directly at cloud base N_{AP}, are given per cubic centimeter. The number reduction is given in percent with respect to the initial number concentrations.

Case	N_d at 200 s	N_d at 600 s	N_d at 1200 s	$N_{AP,nat.,act.}$ (number reduction)	$N_{AP,seeded,act.}$ (number reduction)	Supersaturation peak (%)
Natural	635	420.7	364	855.6 (9.8%)		0.220 677
Natural $\alpha = 0$	921	881.2	807.6	938.9 (10.87%)		0.244 138
C1	969.1	1161	1244	19.5 (0.2%)	970.7 (37.3%)	0.104 34
C2	919.1	971.4	930.9	51.3 (0.6%)	925.2 (61.6%)	0.104 34
C3	742.1	693.3	634.8	115.5 (1.3%)	602.3 (80.3%)	0.104 34
C4	696.7	473.6	417.1	747.2 (8.6%)	152.1 (99.4%)	0.201 07
C4 $\alpha = 0$	1000.9	957.2	610.9	867.2 (10.1%)	149.5 (99.7%)	0.225 363
C4 $\alpha = 0.3$	806.8	640.9	492.1	807.8 (9.3%)	150.8 (99.6%)	0.2164
C4 $\alpha = 0.9$	583	366.1	344.8	639.3 (7.3%)	153.7 (99%)	0.185 08
C5	675.8	442.3	352.35	897.9 (10.3%)	15.21 (99.7%)	0.233 474
C6	696.9	473.7	419.5	747.6 (8.6%)	152 (99.4%)	0.201 177
C7	284.9	350	347.2	166.4 (1.9%)	150 (99.9%)	0.104 34
C8	351	251.6	302.1	243.3 (3.7%)	158.35 (100%)	0.114 466
T1	646.2	399.3	332.7	901 (10.3%)	0.0315 (100%)	0.237 12
T2	665.6	426.1	365.9	906.5 (10.3%)	0.003 15 (100%)	0.238 457
T3	667.4	432.4	354.2	907 (10.4%)	0.000 315 (100%)	0.238 57
T4	667.6	433	365.5	907 (10.4%)	0.000 031 5 (100%)	0.238 58
T5	667.6	433	365.3	906.9 (10.4%)	0.003 15 (100%)	0.238 56
T6	667.5	432	346.2	906.8 (10.3%)	0.003 15 (100%)	0.238 53
T7	667	430.2	347.8	906.7 (10.3%)	0.003 15 (100%)	0.238 496
T8	661.6	414.6	362.5	906.2 (10.3%)	0.003 15 (100%)	0.238 39
S	666.7	430.3	343.5	907 (10.4%)	0.000 089 7 (100%)	0.238 565

simulations concerning warm clouds are summarized in Table 5. The results are also displayed in Fig. 2. Figure 2a displays the time evolution of a drop water mass spectrum forming on a rural aerosol particle spectrum described by Eq. (1) and Table 2. Cloud base, at 1-km altitude, has a temperature of 288 K, and cloud top is at 4.33 km with a temperature of 267 K. Many small drops ($\sim$635 cm^{-3} after 200 s) form at cloud base and grow only little by condensation in the first 1200 s of cloud life. Only after 20 min the second maximum in the liquid water spectrum develops indicating the presence of precipitation-sized drops. The liquid water content then is around 1.2 g m^{-3}.

In Figs. 2b–d we see that seeding the same cloud below cloud base with the seeding spectra given by Eq. (2) and Table 3 significantly accelerates the formation of larger drops in all cases. Table 5 allows understanding the competition between the natural aerosol particles and the seeded particles. In the natural case the peak supersaturation is 0.22% activating 855 cm^{-3} of particles. This represents about 9.8% of the number concentration of the initial natural aerosol population. With time the number concentration of the formed drops decreases due to detrainment and collision and coalescence processes (cf. Table 5).

In the seeded cloud C4, the number of naturally activated aerosol particles decreases (only 747 cm^{-3} corresponding to 8.6% of the initial aerosol population) while a significant number of seeded particles (152 cm^{-3}) were activated. The peak supersaturation has decreased a bit with respect to the natural case (0.2%) due to the presence of the large number of small and large particles. After 200 s the number of drops is a bit larger (697 cm^{-3}) than in the nonseeded case. Figure 2b illustrates that these additional drops, formed on larger aerosol particles, have radii between 10 and 300 μm. These numerous drizzle-size drops collide and coalesce producing precipitation in 20 min (see Fig. 2b and Table 5).

These results were obtained using a mean entrainment rate of $\alpha = 0.6$. In order to quantify the effect of the homogeneous entrainment assumption, we have varied the parameter α. The results are displayed in Fig. 3. In Figs. 3a,b, α was set to zero for the natural and the C4 cases, while Figs. 3c,d show the impact of an even higher entrainment rate than used in Fig. 2. We can state that the main change is effectively caused by the seeding agent, while the entrainment rate plays a relatively small role during the early stages of the cloud.

Figures 4a,b display the consequences of the cloud formation on the interstitial (unactivated) aerosol particle spectrum in the adiabatic case and in the case with an entrainment rate of $\alpha = 0.6$. We see the initial natural and the initial seeded, moist aerosol particle spectrum, and the part that remains after 200 s of cloud lifetime. We see that both spectra are truncated at a radius that corresponds to the activating supersaturation. Furthermore, the natural spectrum has decreased several orders of magnitude at the small particle end due to impaction scavenging by Brownian motion (Flossmann et al. 1985). We note that the entrainment rate only slightly modified the spectra. It replenished some previously

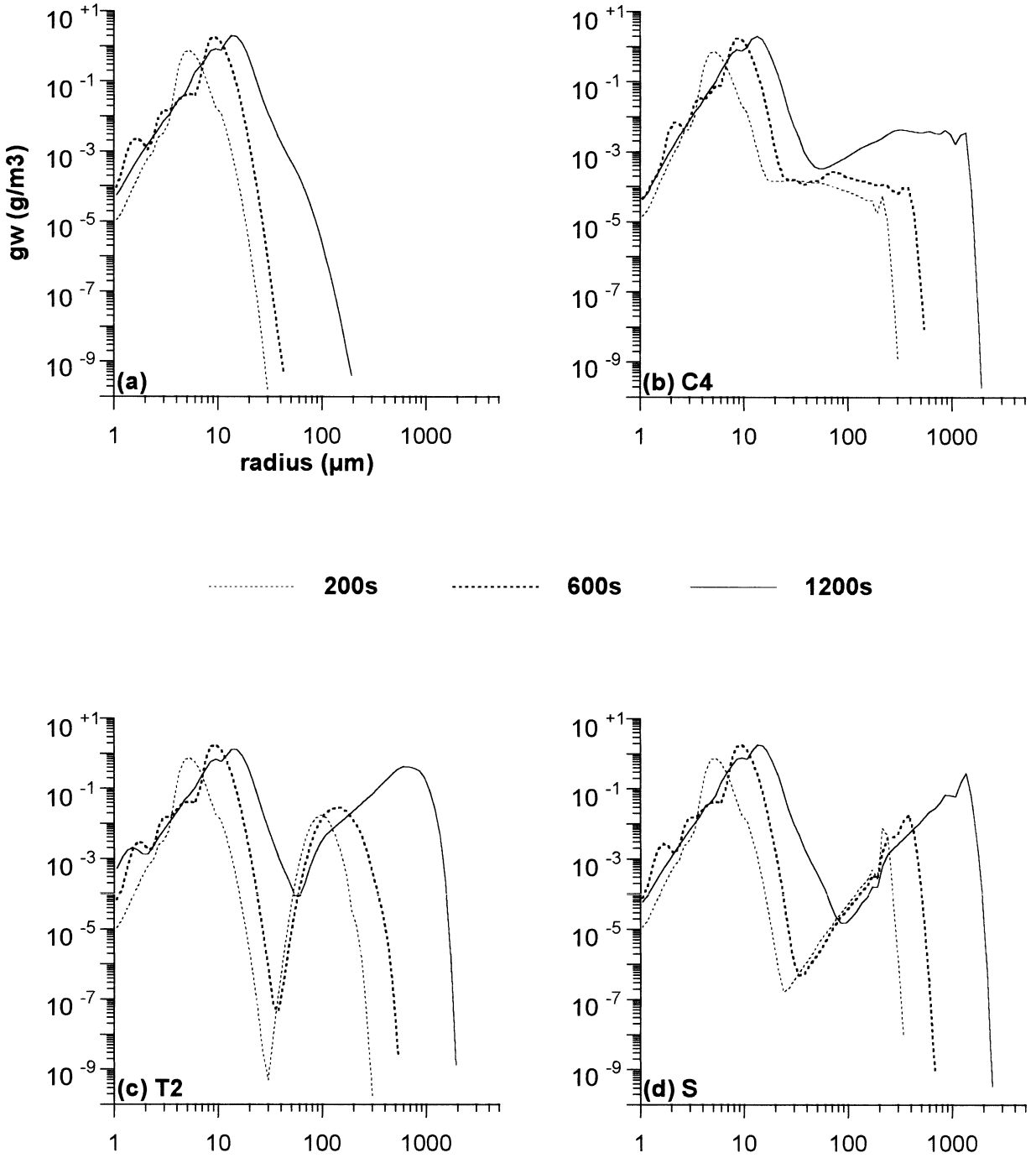

FIG. 2. Drop water mass density distribution function as a function of drop radius and as a function of parcel lifetime (a) for the unseeded case, (b) for case C4 (c), for case T2 and, (d) for case S, for a warm convective cloud, for an entrainment rate of $\alpha = 0.6$.

emptied categories around the activation radius. As, however, the general influence of the entrainment rate at these early cloud stages is small, we will keep for the following the value of $\alpha = 0.6$.

In cases T2 and S, the seeded particles act quite differently, as can be seen from Table 5. Here, very few but giant aerosol particles are activated early. Their uptake of vapor is slow, thus the supersaturation builds up to values of 0.24% activating slightly more natural particles ($\sim$907 cm^{-3} corresponding to 10% of the initial aerosol number concentration) than in the nonseeded case. The few giant seeded particles initiate a rapid precipitation, which is even faster in case T2 (see Fig. 2).

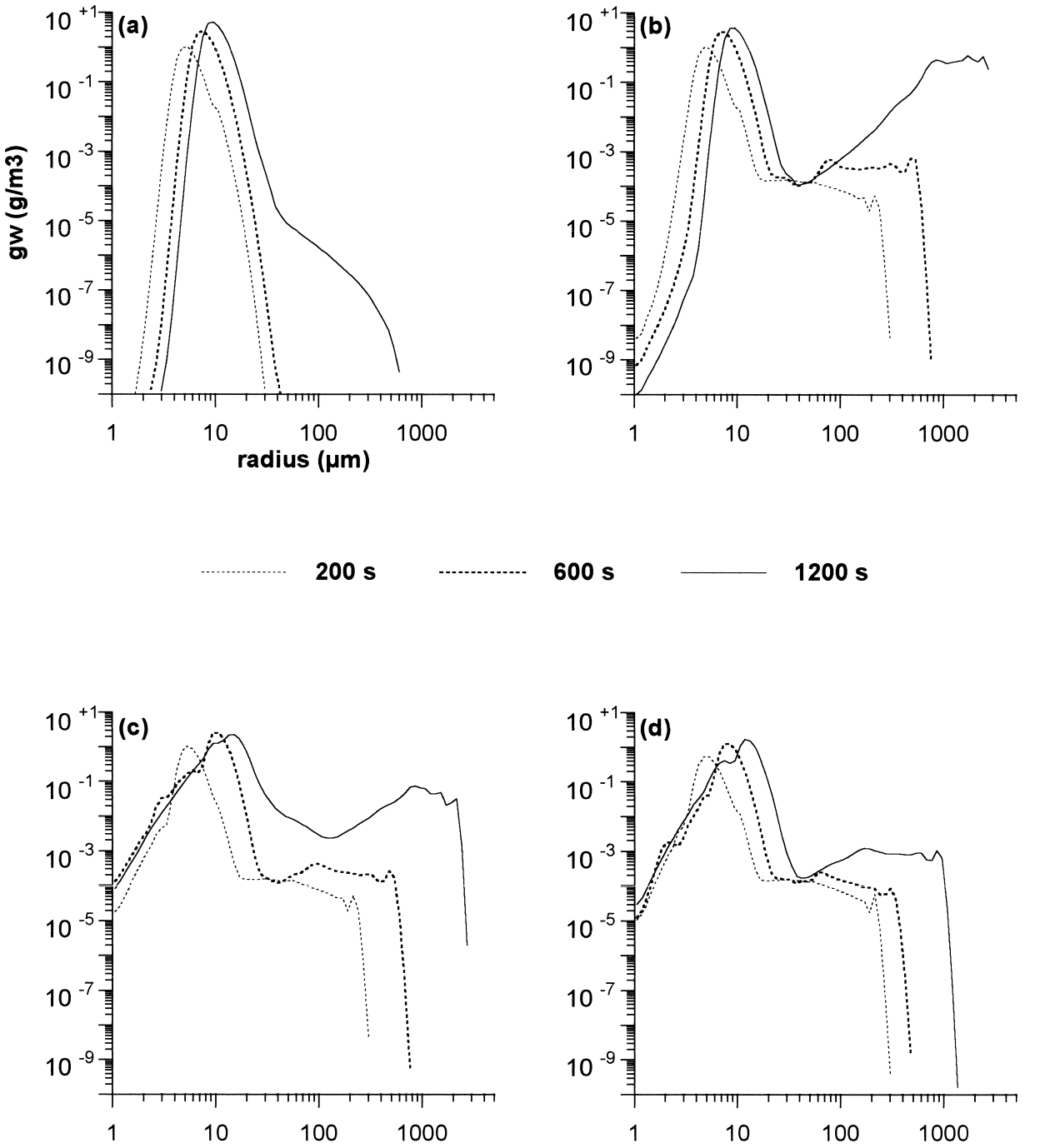

FIG. 3. Drop water mass density distribution function as a function of drop radius and as a function of parcel lifetime (a) for the adiabatic unseeded case, (b) for an adiabatic case C4, (c) for case C4 with $\alpha = 0.3$ and, (d) for case C4 with $\alpha = 0.9$, for a warm convective cloud.

However, as already pointed out by CBM97, this rapid production of large drops might result in a premature precipitation limiting the seeding effect to the seeded cloud-region alone while seeding with flares, as is case C4, results initially in an increase in the drizzle-size drops. These numerous drizzle-size drops are probably small enough to stay inside the cloud for a longer time, propagate to larger regions and, thus, initiate precipitation in the entire cloud. We can, thus, confirm the production by the flares of these drizzle-size drops, and will devote an increased attention to the flare cases.

In the following, we will present sensitivity studies concerning the number concentration of seeding particles and their mean radius. We will focus here on the spectra of CBM97 and TRL94, as the SS96 spectrum is of less interest given the conclusions above.

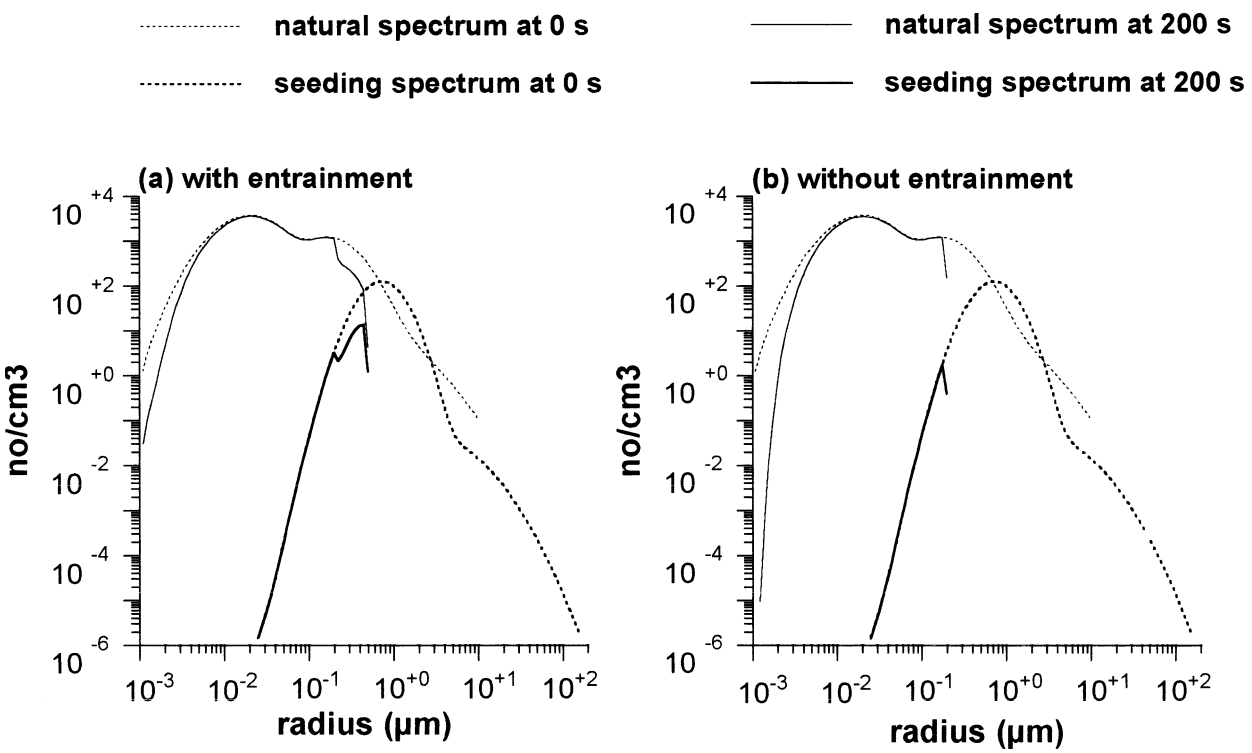

FIG. 4. Moist aerosol particle number concentration for (a) the case C4 with $\alpha = 0.6$ and (b) the adiabatic case C4. The dotted lines represent the aerosol particle spectra at $t = 0$; the solid lines give the unactivated particles at $t = 200$ s.

a. Results of the sensitivity tests concerning the seeding spectrum according to CBM97

With cases C1–C5 (see Table 4), we performed a sensitivity test concerning the number concentration of the two modes of seeding particles. The ratio of the concentrations for the two lognormal distributions was selected to be $1{:}7 \times 10^{-4}$ based on Fig. 1 of CBM97 and YLRT00. Looking at Table 5, we note that for very high numbers of seeded particles (e.g., case C1, Fig. 5a), the seeded particle spectrum dominates over the natural one. Fewer than 0.2% of the natural number of particles were activated but 37% of the seeded particles were activated. As those drops were rather large, the supersaturation peak decreased. When the number of seeded particles decreases (cases C2–C5) the number of activated seeded particles decreases also and correspondingly the number of natural particles increases in such a way that the total number of drops varies only slightly (cases C1, C2, and C3). Thus, we can identify a kind of saturation of the seeding effect linked to the increase in the number of seeded particles. It might be possible, however, that this saturation effect is introduced by the parcel model dynamics and will be different in a more complex dynamic framework. Furthermore, the model results indicate that too low a number concentration of seeding particles, as represented by case C5 (Fig. 5b), does not seem satisfactory since it leads to precipitation formation only very late, almost as in the unseeded case (Fig. 2a). Thus, concerning the number concentrations, the case C4 seems to represent the optimum as it increases the number of drizzle-sized drops without producing rain drops too rapidly.

In the following we studied the effect of the mean particle radius. In order to make this dependency appear more clear we restricted the seeded spectrum to a unimodal one, as suggested by CBM97. The mean radius of the distributions moves from 0.15 (case C6 corresponding to the location of the first mode in C4), to 0.5 (case C7 corresponding to the second mode in C4), and beyond to 1.25 (case C8), to study the effect of even larger seeding particles. The number concentration was chosen to be identical in all cases, corresponding to the optimum identified above for C4. The extremes of this study are summarized in Figs. 3c, d. We see there that the result of case C6 (Fig. 5c) closely resembles the unseeded evolution (see Fig. 2a), even though the numbers in Table 5 are almost the same as in case C4. This is due to the fact that the seeded spectrum covers the same size range as the natural background spectrum (rural type) and is missing the tail of a small number of large particles as in case C4. Thus, no larger drops are formed and, as the natural spectrum was already not favorable for precipitation formation, the seeding does not improve the situation.

As the mean radius of the seeded spectrum increases,

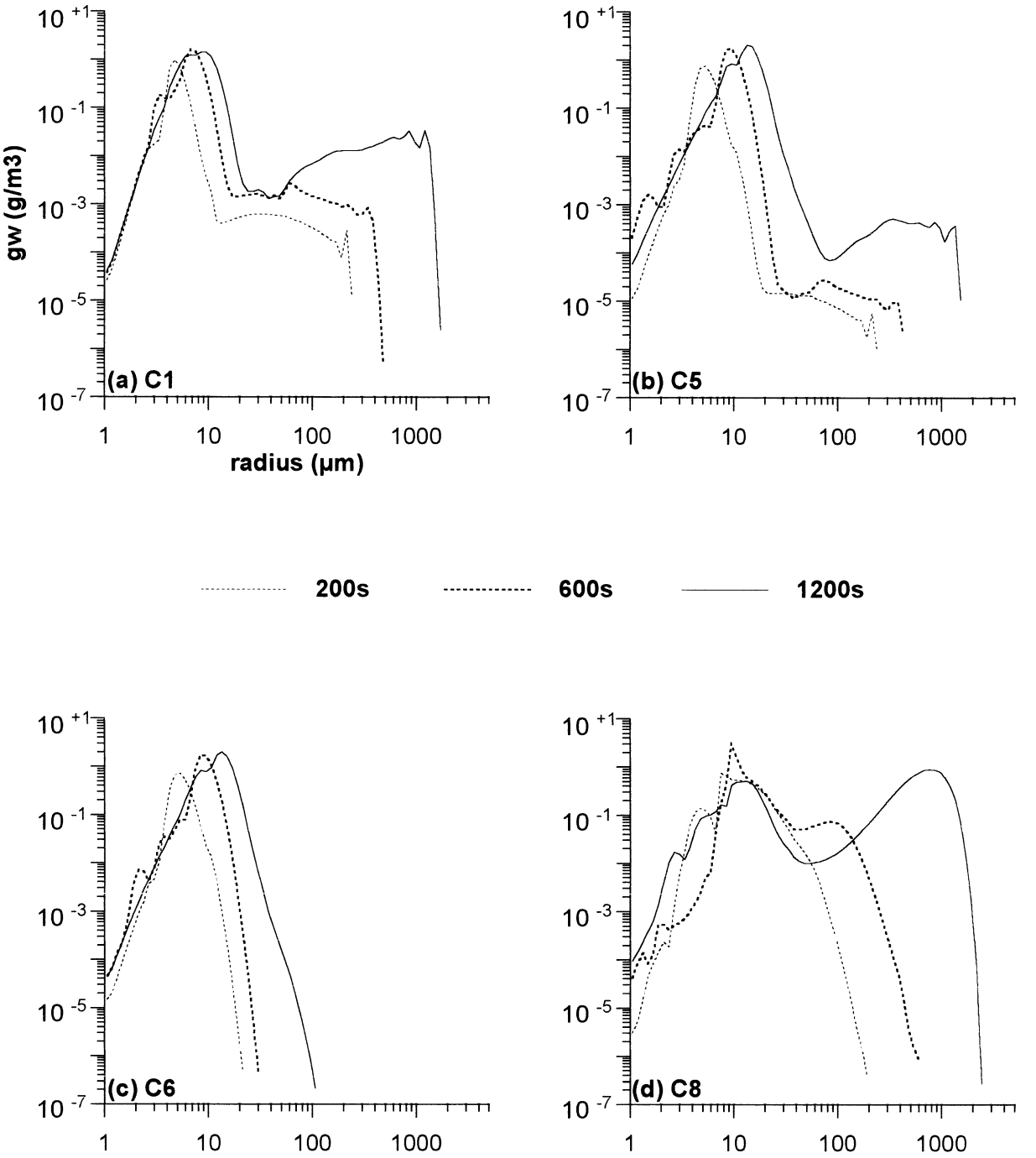

FIG. 5. Drop water mass density distribution function as a function of drop radius and as a function of parcel lifetime (a) for case C1, (b) for case C5, (c) for case C6, and (d) for case C8, for a warm convective cloud.

the efficiency for rain production increases. This effect is almost continuous. We can, thus, conclude that the largest mean radius corresponding to case C8 would represent the most rapid production of raindrops. By continuing the sensitivity tests for the spectrum of Tzivion et al. (1994), we will see whether this evolution will confirm itself for even larger salt crystals.

b. Results of the sensitivity tests concerning the seeding spectrum according to TRL94

The results of sensitivity studies with the spectrum according TRL94 are displayed in Fig. 6 and Table 5. In the first set of tests the mean radius stayed constant; only the total number concentration increased in each

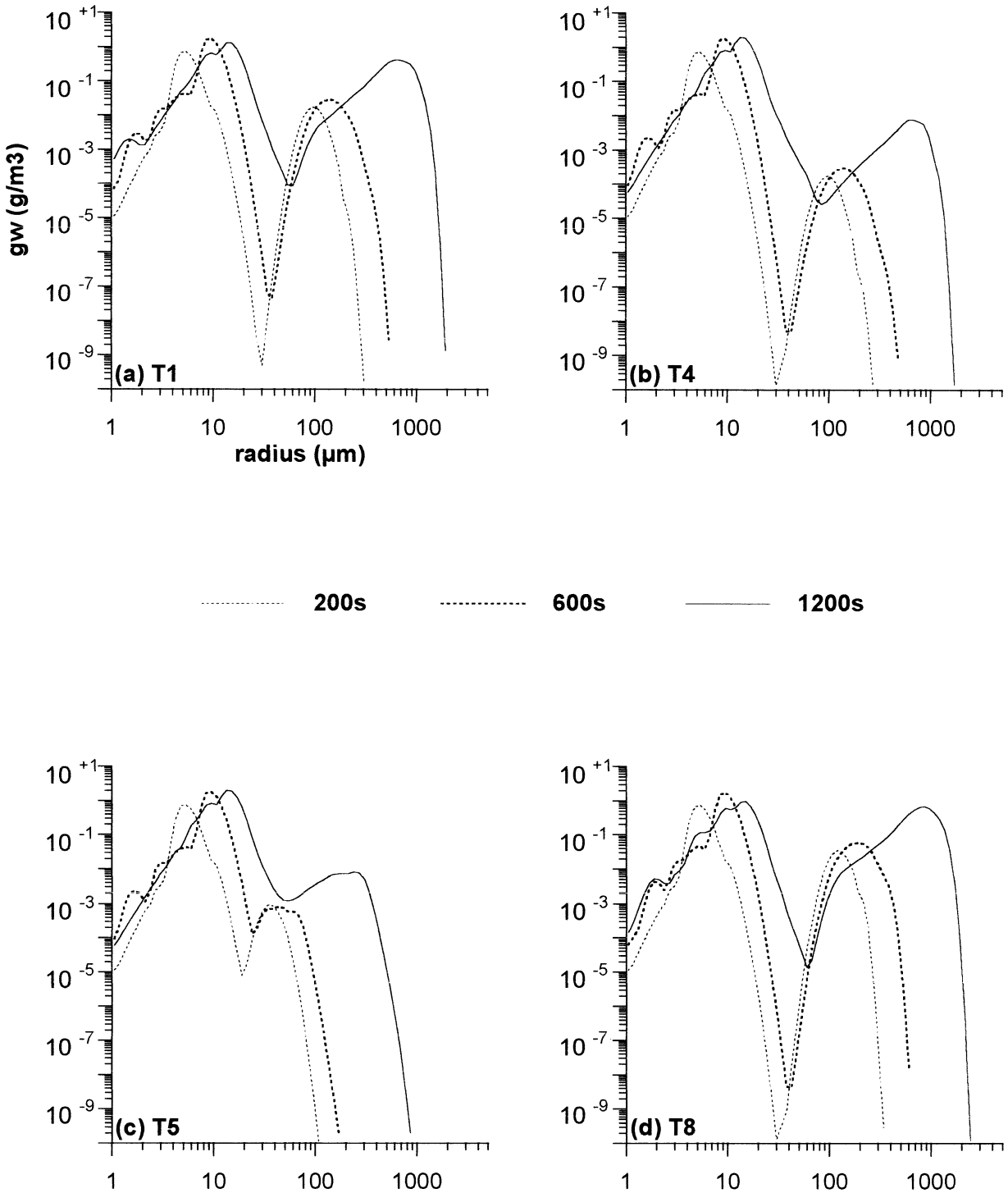

FIG. 6. Drop water mass density distribution function as a function of drop radius and as a function of parcel lifetime (a) for case T1, (b) for case T4, (c) for case T5, and (d) for case T8, for a warm convective cloud.

test, by a factor of 10 (cases T1–T4). Figures 6a,b display the results of the two extreme cases T1 and T4. Similar to the cases of CBM97, we can detect a kind of saturation of the seeding effect. Comparing T1, T2, and T3, only little enhancement of precipitation formation can be noted.

Concerning the increase in radius from cases T5 to T8 we can see (Fig. 6c,d) an enhancement of precipi-

tation production the larger the mean radius gets, in line with the findings for the C-cases. However, this enhancement is not improving rain formation significantly further, once $r > 10$ μm. In addition to that, we can see from Fig. 4c that the case T5, with a mean radius of 6 μm, produces results similar to C4 regarding the number concentration of drizzle-size drops. Thus, the T-sensitivity studies allow us to define the optimum range of the mean radius of the seeding particles between 0.5 (from C4) and 6 (from T5) μm, for the dynamical case studied.

In the following section we will extend our study to the early stages of mixed-phase clouds to see whether seeding by hygroscopic flares would also be an interesting approach for such clouds.

5. Results of the sensitivity test for mixed-phase clouds

Because of the need to simulate lower temperatures inside the cloud than in warm clouds, the sounding was changed for this case study. The temperature of cloud base at 750 m is 279 K and the temperature at cloud top at 4.9 km is 247 K. The unseeded cloud again forms on a rural aerosol particle spectrum as given by Eq. 1 and Table 2. As the cloud evolves a narrow drop size spectrum has again formed, displayed in Fig. 7a. Similarly to the warm case (Fig. 2a) the drop size broadens little due to collision and coalescence as the liquid water content increases to 1.1 g m^{-3} at 20 min (Table 6). Then, the cloud top extends into sufficiently cold regions that an important number of ice crystals (Fig. 8a) and graupel (Fig. 9a) form, due to Bigg freezing of drops. Thus, the liquid water content of the drops starts to decrease and at 1800 s we see a noticeable reduction in water mass associated with the drop spectrum (Fig. 7a). Thus, raindrops will not be formed via the liquid phase. However, after 30 min an important number of graupel particles between 1 and 9 mm appear that continue to grow slowly.

In the model we have seeded the cloud with the three hygroscopic seeding spectra discussed above (C4, T2, S). The trend indicated already in the study of warm clouds is confirmed. With increasing size of the seeding particles the liquid drop spectrum activates the collision and coalescence process earlier in the cloud lifetime (Figs. 7b–d) even though the number of drops initially formed is almost the same (cf. Tables 5 and 6). The most rapid development can be noted again for the case S that has produced millimeter-sized drops after 20 min. In the seeded cloud the formed large drops freeze and an increasing number of graupel (Figs. 9b–d) appear. These ice particles reduce the number and size of the liquid drops so that near cloud top almost no drizzle-sized drops remain. The ice crystal spectra that appear (Figs. 8b–d) are almost identical to the ones formed in the unseeded case (Fig. 8a). These have been formed by the freezing of small drops that are practically untouched by the seeding. However, the number of graupel particles between 1 and 9 mm has significantly increased in all cases. In fact, this result suggests that again the seeding will increase the number of large hydrometeors, which will eventually fall out and reach the ground as liquid or solid depending on the height of the 0° isotherm.

With regard to the mixed-phase clouds we have effected the same kinds of sensitivity tests concerning the seeding agents, their size distribution, and their number concentration (see Flossmann et al. 1999). However, they will not be presented here, as they do not reveal any additional information.

6. Discussion

We have applied a microphysical model (DESCAM) coupled with a parcel dynamics to study the impact of hygroscopic seeding on the early stage of the evolution of a warm and a mixed-phase convective cloud. The microphysical model allows calculation of the time evolution of the drop, the ice crystal, and the graupel spectra, and considers nucleation on an aerosol particle spectrum, explicitly. Even though DESCAM was developed to calculate particle and gas scavenging, it is, due to its explicit configuration, very much adapted to study the evolution of a cloud that forms on a natural background particle spectrum as well as on artificially introduced seeding particles. These seeding particles enter into competition with the natural particles, and the relative size and number distributions of both finally determine the evolution of the cloud. More specifically we have found the following.

1) Clouds that form on a maritime type aerosol particle spectrum favorable to a rapid onset of the collision–coalescence process form rain easily and are, thus, not useful seeding candidates. At the worst, seeding can reduce rain, when the added particles are too numerous and in the same size range as the background aerosol. (The figures were not shown here).
2) The clouds most sensitive to seeding are the ones that form on rural-type aerosol particle distributions, just at the limit of conditions suitable for the onset of natural precipitation formation. Thus, we selected such a case for our sensitivity study.
3) For the study presented here we used an entraining air parcel model. Thus, the results obtained have to be discussed in this dynamical framework. However, the actual parameterization of the entrainment rate has a relatively small influence on the presented results as we limit our discussion to the early stages of a cloud where the influence of entrainment is generally small. The major impact on the hydrometeor spectra results from the chosen natural and seeded aerosol particle spectra.
4) In order to initiate or accelerate precipitation formation the seeding particles have to be larger than

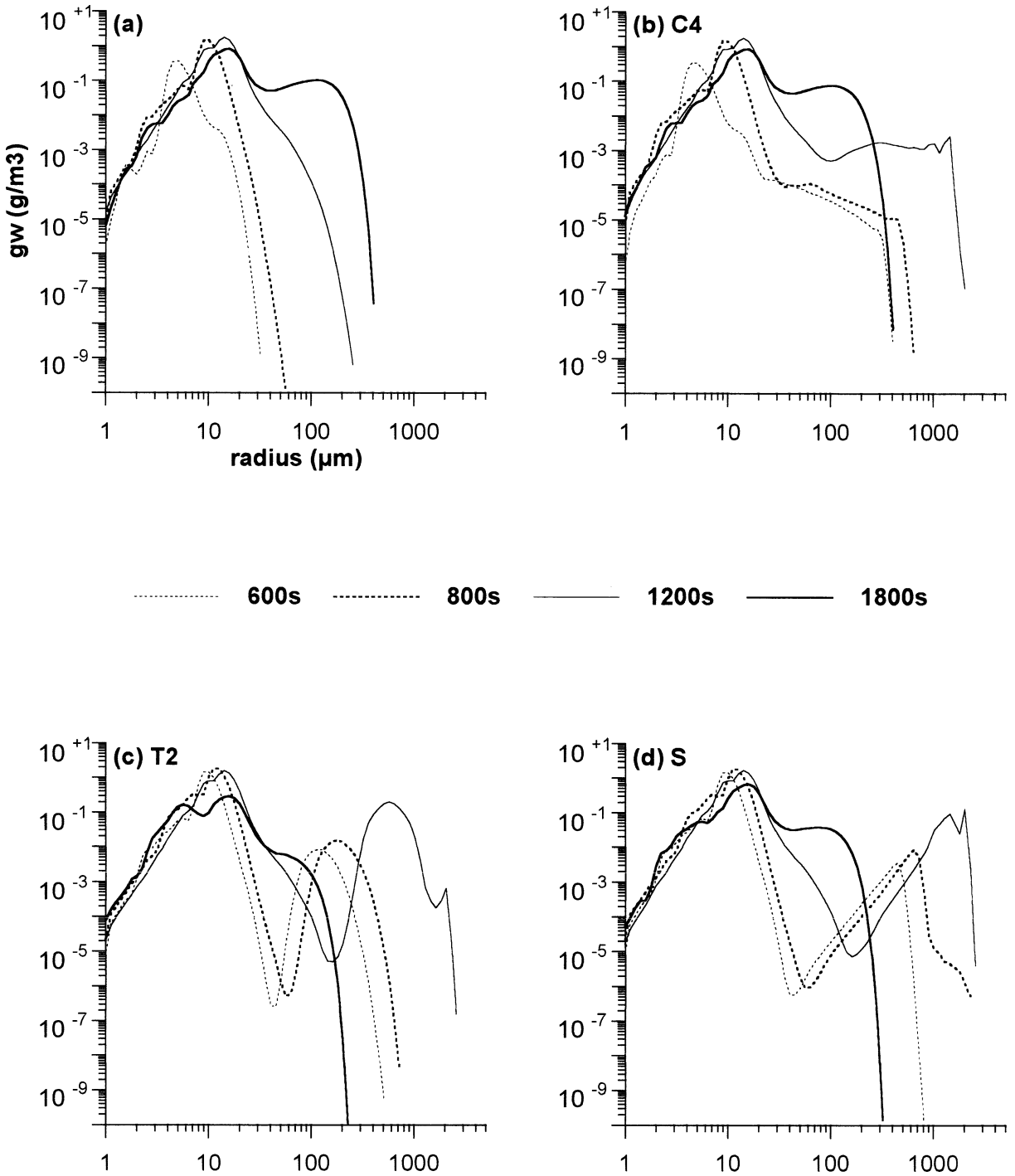

FIG. 7. Drop water mass density distribution function as a function of drop radius and as a function of parcel lifetime (a) for the unseeded case, (b) for case C4, (c) for case T2, and (d) for case S for a mixed-phase convective cloud.

the natural ones. In this configuration they take over the role of principal nuclei and reduce the number of activated background particles.

The findings in 1, 2, and 4 are in agreement with YLRT00, CBM97, TRL94, and SS96.

5) The acceleration of precipitation formation is greater the larger the seeded particles. Thus, the most rapid formation occurred in the model for very large radii (>15 μm). However, the precipitation particles that form on these ultragiant condensation nuclei might fall out prematurely. Thus, the seeding will act only

TABLE 6. Results as a function of time for mixed-phase clouds for the unseeded case (natural) and the three seeded cases from Table 3. Parameters N_d, N_i, and N_g are the number concentrations for drops, ice crystals, and graupel particles, respectively, per cubic centimeter; W_d, W_i, and W_g are the condensed mass of drops, ice crystals, and graupel, respectively, in grams per cubic meter. Here S_{peak} is the peak supersaturation.

Case		200 s	600 s	800 s	1200 s	1800 s
Natural S_{peak}: 0.28%	N_d	335.2	286.9	348.9	236.4	126.7
	N_i	0.0	4.176×10^{-9}	1.18×10^{-7}	3.712×10^{-5}	5.21×10^{-2}
	N_g	0.0	0.0	0.0	5.231×10^{-10}	4.532×10^{-2}
	W_1	0.161	0.64	0.943	1.112	0.749
	W_i	0.0	2.019×10^{-11}	2.463×10^{-9}	3.637×10^{-6}	1.125×10^{-2}
	W_g	0.0	0.0	0.0	2.617×10^{-9}	0.128
C4 S_{peak}: 0.24%	N_d	358.9	300.7	375.1	242.5	131.5
	N_i	0.0	4.709×10^{-9}	1.18×10^{-7}	3.717×10^{-5}	5.516×10^{-2}
	N_g	0.0	1.584×10^{-13}	1.41×10^{-11}	7.47×10^{-8}	3.315×10^{-3}
	W_1	0.164	0.64	0.943	1.112	0.727
	W_i	0.0	1.955×10^{-11}	2.432×10^{-8}	3.604×10^{-5}	0.011
	W_g	0.0	1.118×10^{-12}	1.548×10^{-9}	1.405×10^{-4}	0.167
T2 S_{peak}: 0.28%	N_d	334.7	285.4	345.9	214.2	263.9
	N_i	0.0	4.612×10^{-9}	1.14×10^{-7}	3.336×10^{-5}	0.102
	N_g	0.0	3.308×10^{-11}	9.741×10^{-10}	2.712×10^{-6}	4.81×10^{-4}
	W_1	0.165	0.64	0.941	1.1195	0.306
	W_i	0.0	2.685×10^{-11}	2.372×10^{-9}	3.35×10^{-6}	8.233×10^{-3}
	W_g	0.0	3.509×10^{-10}	3.205×10^{-8}	2.578×10^{-3}	0.64
S S_{peak}: 0.28%	N_d	334.75	286.2	347.5	229	204.8
	N_i	0.0	4.692×10^{-9}	1.17×10^{-7}	3.581×10^{-5}	8.664×10^{-2}
	N_g	0.0	1.021×10^{-11}	3.319×10^{-10}	1.23×10^{-6}	2.865×10^{-3}
	W_1	0.162	0.64	0.94	1.127	0.558
	W_i	0.0	2.008×10^{-11}	2.441×10^{-9}	3.548×10^{-6}	1.211×10^{-2}
	W_g	0.0	2.495×10^{-9}	2.454×10^{-7}	1.998×10^{-2}	0.353

in the immediate vicinity of the seeding location. The problem of the premature fallout of the seeded drops has been noted before and, thus, the importance of the Langmuir chain reaction (Farley and Chen 1975; Biwas and Dennis 1971) and the collisional breakup process (Tzivion et al. 1994) have been pointed out to lengthen and widen the effect of the hygroscopic seeding or it has been proposed to seed from cloud top (Rasmussen et al. 1989). In this respect we can support the statement of CBM97 who found that seeding with flares probably will improve this situation by the fact that the small particles emitted by the hygroscopic flares will not immediately increase the number of rain drops but, instead, initially increase the number of drizzle-sized drops. Those will not fall out as rapidly and have, thus, a greater chance to be diffused throughout the cloud and initiate collision–coalescence in the entire cloud region. This theory seems plausible; however, it has yet not been confirmed by measurements.

6) As to the saturation of the seeding effect for increasing number concentration, this result has not been reported before. This is probably due to the fact that previous models were not able to fully take into account the competition between the nuclei of different size and origin. Our model results suggest that the cloud selects the largest possible nuclei and then stops activation. As long as the seeding agent displays no extremes (very small or very large particles) in the distribution function the formed cloud will be rather insensitive to overseeding. Here, however, the impact of the parcel model dynamics has to be quantified. Still, underseeding is possible as already pointed out by other studies.

The above are the main conclusions we can draw for the hygroscopic seeding of warm, that is, all-liquid clouds. Concerning the mixed-phase convective clouds we can conclude the following.

7) Again, hygroscopic seeding with flares or particles increases the formation of large drops. If we assume that ice initiation in a convective cloud mainly works via the Bigg freezing of drops, this will result in an increase of the number of ice particles in the millimeter-sized range. At the same time the available liquid water decreases without affecting the concentration of small ice crystals. The graupel particles will then grow and precipitate, either in a solid or a liquid form. Thus, also in the mixed-phase cloud, the hygroscopic seeding has accelerated the precipitation formation.

7. Conclusions

From the results of the case studies presented above we conclude that hygroscopic seeding by flares represents a promising approach for the future. From practical considerations (weight, easy handling) hygroscopic flares have advantages with respect to classical hygroscopic seeding techniques.

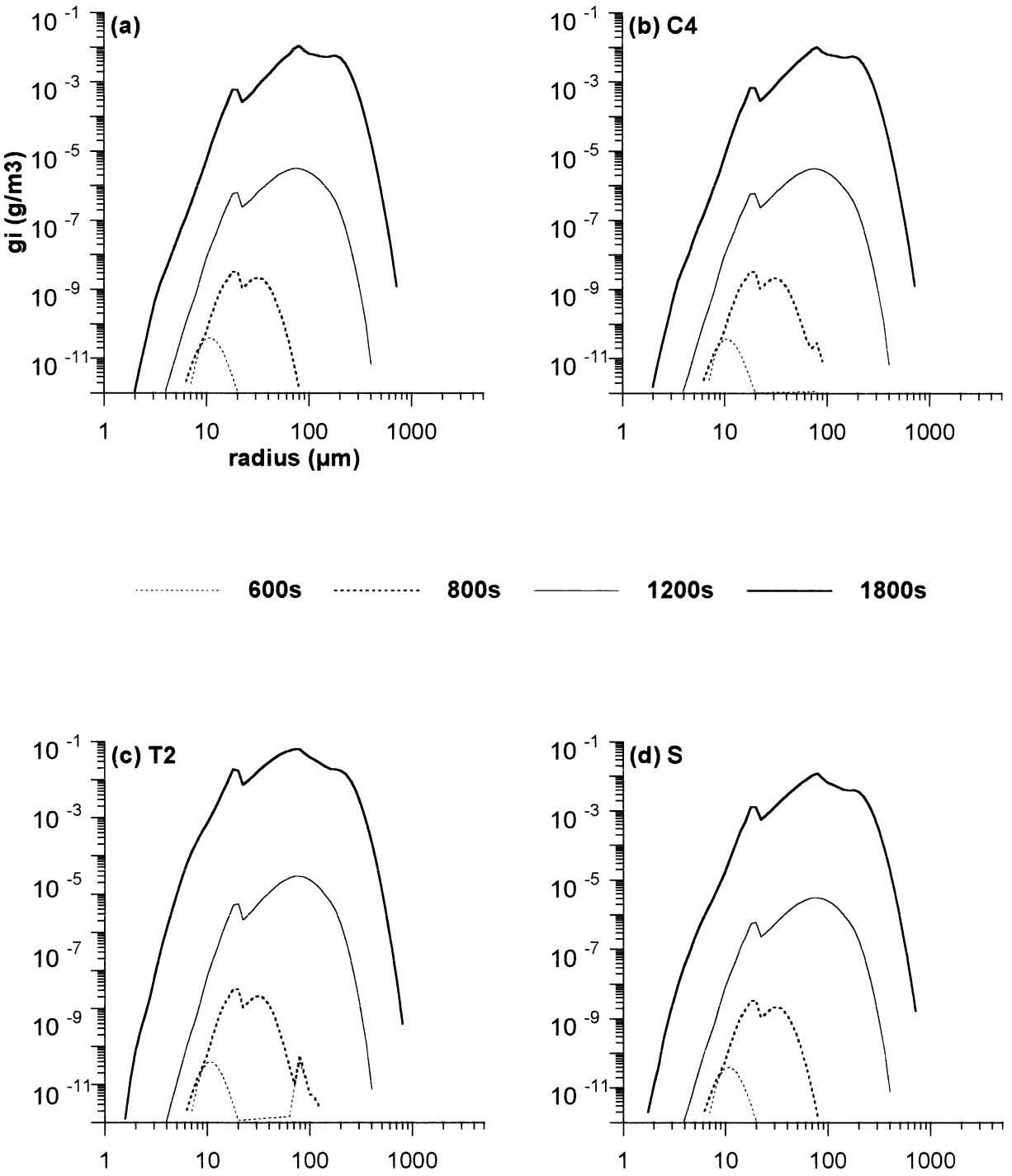

FIG. 8. Ice crystal mass density distribution function as a function of ice crystal radius and as a function of parcel lifetime (a) for the unseeded case, (b) for case C4, (c) for case T2, and (d) for case S, for a mixed-phase convective cloud.

The modeling study supports this choice. Smaller seeding particles have the advantage of increasing the number of drizzle-sized drops, increasing the chance of the seeding material to stay in the cloud and to affect the whole cloud. Larger salt crystals, though increasing precipitation production in the model, risk a premature precipitation. Concerning the radius, we can conclude that mean radii between 0.5 and 6 μm would be desirable to get a good seeding effect, for the dynamical case studied.

For the first time we carried out a spectral modeling study with a detailed treatment of the aerosol particle

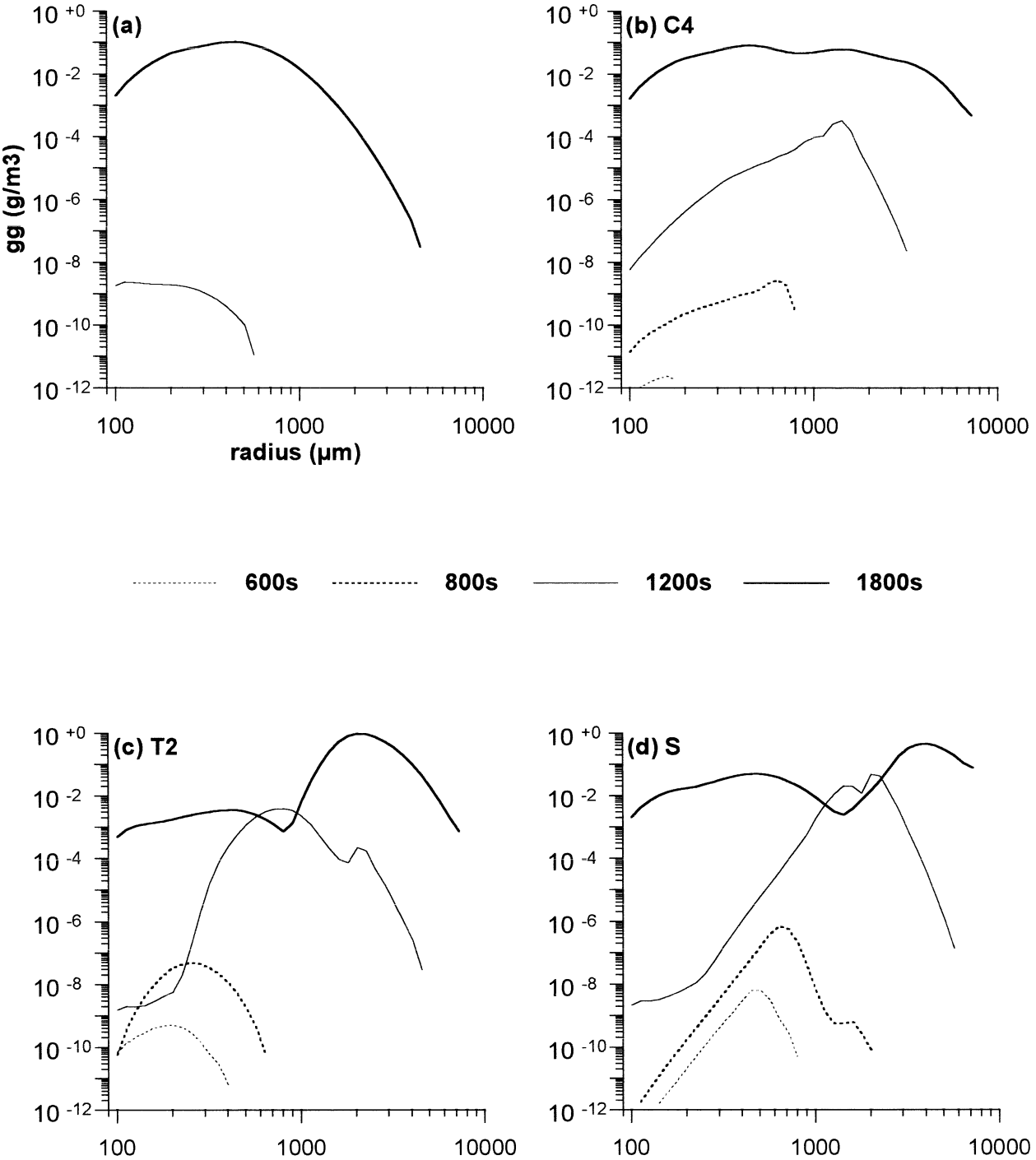

FIG. 9. Graupel mass density distribution function as a function of graupel particle radius and as a function of parcel lifetime (a) for the unseeded case, (b) for case C4, (c) for case T2, and (d) for case S for a mixed-phase convective cloud.

spectra concerning the potential of hygroscopic flares for treating mixed-phase clouds. Even though the applicability of the model is limited to the initial phase of graupel formation, the results are, nevertheless, encouraging, in terms of a potential impact of flare seeding also for a precipitation increase in mixed-phase clouds.

Certainly, the results presented here are not final. They give an indication as to the possible effect a hygroscopic seeding might have in the early stages of convective cloud development. Thus, to verify and generalize these suggested impacts, modeling studies must be extended to consider the 3D structure of the cloud, with

horizontal shear, updrafts and downdrafts, and precipitation. Then, certainly the model output can be compared with results of field campaigns to be able to finally judge the performance of hygroscopic flares in the increase of liquid precipitation or even for the reduction of hail.

Acknowledgments. The authors acknowledge with gratitude the financial support provided by the Centro Servizi Agrometeorologici per il Friuli-Venezia Guilia (CSA.) in Cervignano del Friuli, Italy, under the responsibility of G. M. Morgan, Jr. The authors are also grateful for the help of G. M. Morgan, Jr. during the preparation of the manuscript, as well as for the comments of an anonymous reviewer. The calculations for this paper have been done on the Cray C98 and C94 of the Institut du Développement et des Ressources en Informatique Scientifique (IDRIS–CNRS) in Orsay, France, under Project 940180. The authors acknowledge with gratitude the hours of computer time and the support provided.

REFERENCES

Ackerman, A. S., O. B. Toon, and P. V. Hobbs, 1995: Numerical modeling of ship tracks produced by injections of cloud condensation nuclei into marine stratiform clouds. *J. Geophys. Res.,* **100,** 7121–7133.

Ahr, M., A. I. Flossmann, and H. R. Pruppacher, 1989: On the effect of the chemical composition of atmospheric aerosol particles on nucleation scavenging and the formation of a cloud interstitial aerosol. *J. Atmos. Chem.,* **9,** 465–478.

Alheit, R. R., A. I. Flossmann, and H. R. Pruppacher, 1990: A theoretical study of the wet removal of atmospheric pollutants. Part IV: The uptake and redistribution of aerosol particles through nucleation and impaction scavenging by growing cloud drops and ice particles. *J. Atmos. Sci.,* **47,** 870–887.

Baker, M. B., and J. Latham, 1979: The evolution of droplet spectra and rate of production of embryonic rain drops in small cumulus clouds. *J. Atmos. Sci.,* **36,** 1612–1615.

——, and ——, 1982: Diffusive model of the turbulent mixing of dry and cloudy air. *Quart. J. Roy. Meteor. Soc.,* **108,** 871–898.

——, R. G. Corbin, and J. Latham, 1980: Influence of entrainment on the evolution of cloud droplet spectra, Pt. 1, Model of inhomogeneous mixing. *Quart. J. Roy. Meteor. Soc.,* **106,** 581–598.

Bigg, E. K., 1953: The formation of atmospheric ice crystals by the freezing of droplets. *Quart. J. Roy. Meteor. Soc.,* **79,** 510–519.

Biwas, K. R., and A. S. Dennis, 1971: Formation of a rain shower by salt seeding. *J. Appl. Meteor.,* **10,** 780–784.

Cooper, W. A., R. T. Bruintjes, and G. K. Mather, 1997: Calculations pertaining to hygroscopic seeding with flares. *J. Appl. Meteor.,* **36,** 1449–1469.

Farley, R. D., and C. S. Chen, 1975: A detailed microphysical simulation of hygroscopic seeding on the warm rain process. *J. Appl. Meteor.,* **14,** 718–733.

Federer, B., and Coauthors, 1986: Main results of Grossversuch IV. *J. Climate. Appl. Meteor.,* **25,** 917–957.

Flossmann, A. I., 1991: The scavenging of two different types of marine aerosol particles using a two-dimensional detailed cloud model. *Tellus,* **43B,** 301–321.

——, 1994: A 2-D spectral model simulation of the scavenging of gaseous and particulate sulfate by a warm marine cloud. *J. Atmos. Res.,* **32,** 255–268.

——, W. D. Hall, and H. R. Pruppacher, 1985: A theoretical study of the wet removal of atmospheric pollutants. Part I: The redistribution of aerosol particles captured through nucleation and impact scavenging by growing cloud drops. *J. Atmos. Sci.,* **42,** 583–606.

——, H. R. Pruppacher, and J. H. Topalian, 1987: A theoretical study of the wet removal of atmospheric pollutants. Part II: The uptake and redistribution of $(NH_4)_2\ SO_4$ particles and SO_2 gas simultaneously scavenged by growing cloud drops. *J. Atmos. Sci.,* **44,** 2912–2923.

——, J. Thielen, W. Wobrock, B. Boudevillain, and D. Caro, 1999: Final project report: State of the art of the modelling of hail modification. Tech. Report, 119 pp. [Available from LaMP, Université Blaise Pascal, 63177 Aubiére, France.]

Foote, G. R., and C. A. Knight, 1979: Results of a randomized hail suppression experiment in northeast Colorado. Part I: Design and conduct of the experiment. *J. Appl. Meteor.,* **18,** 1526–1537.

Jaenicke, R., 1988: Aerosol physics and chemistry. *Landolt-Boernstein: Zahlenwerte und Funktionen aus Naturwissenschaften und Technick,* V 4b, G. Fischer, Ed., Springer, 391–457.

Knight, C. A., and P. Squires, Eds.,1982: *Hailstorms of the Central High Plains.* Vol. 1. *The National Hail Research Experiment.* Colorado Associated University Press, 282 pp.

Lee, I. Y., G. Hänel, and H. R. Pruppacher, 1980: A numerical determination of the evolution of cloud drop spectra due to condensation on natural aerosol particles. *J. Atmos. Sci.,* **37,** 1839–1853.

Mather, G. K., 1991: Coalescence enhancement in large multicell storms caused by the emissions from a Kraft paper mill. *J. Appl. Meteor.,* **30,** 1134–1146.

——, D. E. Terblanche, F. E. Steffens, and L. Fletcher, 1997: Results of the South African cloud-seeding experiments using hygroscopic flares. *J. Appl. Meteor.,* **36,** 1433–1447.

Morgan, G. M., Jr., 1973: A general description of the hail problem in the Po Valley of northern Italy. *J. Appl. Meteor.,* **12,** 338–353.

Orville, H. D., and F. J. Kopp, 1977: Numerical simulation of the history of a hailstorm. *J. Atmos. Sci.,* **34,** 1596–1618.

Pruppacher, H. R., and J. D. Klett, 1997: *Microphysics of Clouds and Precipitation.* 2d ed. Kluwer Academic, 954 pp.

Rasmussen, R., B. Silverman, T. Clark, and W. Hall, 1989: Evaluation of seeding effects of tropical clouds using cloud models. *Proc. Fifth WMO Scientific Conf. on Weather Modification and Applied Cloud Physics,* Beijing, China, WMO, 209–212.

Reisin, T., S. Tzivion, and Z. Levin, 1996: Seeding convective clouds with ice nuclei and hygroscopic particles: A numerical study using a model with detailed microphysics. *J. Appl. Meteor.,* **35,** 1416–1434.

Silverman, B. A., and W. Sukarnjanaset, 1996: On the seeding of tropical convective clouds for rain augmentation. Preprints, *13th Conf. on Planned and Inadvertent Weather Modification,* Atlanta, GA, Amer. Meteor. Soc., 52–59.

Sulakvelidze, G. K., and V. V. Tsykunov, 1974: Progress of hail suppression work in the U.S.S.R. *Weather and Climate Modification,* W. N. Hess, Ed., John Wiley and Sons, 410–431.

Tzivion, S., T. Reisin, and Z. Levin, 1994: Numerical simulation of hygroscopic seeding in a convective cloud. *J. Appl. Meteor.,* **33,** 252–267.

Yin, Y., Z. Levin, T. Reisin, and S. Tzivion, 2000: Seeding convective clouds with hygroscopic flares: Numerical simulations using a cloud model with detailed microphysics. *J. Appl. Meteor.,* **39,** 1460–1472.